Appl. Phys. B 79, 741–749 (2004)
DOI: 10.1007/s00340-004-1610-7

Applied Physics B
Lasers and Optics

Z. ALAHMED
R. GUPTA✉

Theory of two-photon photothermal deflection spectroscopy in stationary and flowing media for arbitrary optical pulse length

University of Arkansas, Fayetteville, AR 72701, USA

Received: 21 May 2004/Revised version: 6 July 2004
Published online: 25 August 2004 •

ABSTRACT A general theory of pulsed two-photon photothermal deflection spectroscopy (PTDS) is presented. We find that there are significant enough differences in the amplitude and temporal evolution of PTDS signals between the results of the single- and two-photon theories that if one tries to interpret two-photon data with single-photon theory, the extracted values may be considerably in error. Our theory is sufficiently general that it incorporates both stationary and flowing media and considers optical pulses of arbitrary length. Moreover, the temporal profile of the optical pulse is explicitly taken into account. The two-photon absorption coefficient is explicitly expressed in terms of oscillator strengths and Clebsch–Gordan coefficients, and the Doppler width for both co-propagating and counter-propagating beams is taken into account. Although the theory is primarily developed for atomic and molecular vapors, it can easily be adapted for condensed matter by expressing the absorption coefficient in terms of the properties of the liquid or solid under investigation.

PACS 82.80.Kq; 42.62.Fi; 39.30.+w

1 Introduction

Over the past two decades photothermal spectroscopy has developed into one of the major applied spectroscopic techniques. The technique has been applied to many diverse areas, such as analytical chemistry, semiconductor diagnostics, non-destructive evaluation, materials and surface studies, and medical, biological, and agricultural sciences, to name just a few [1]. Basically, photothermal spectroscopy and its sister technique, photoacoustic spectroscopy [1], are used when fluorescence techniques are inappropriate. In this article, we present a systematic and comprehensive study of the theory of two-photon photothermal deflection spectroscopy (PTDS), which will extend the range of applications of PTDS considerably. For example, the theory presented in this paper will enable quantitative analysis of two-photon PTDS signals obtained from species, such as atomic hydrogen and oxygen, in a combustion environment or in a reacting atmospheric-pressure plasma. Although this theory is primarily developed for atomic and molecular vapors, it is also applicable to liquids and solids.

The principle of the photothermal technique is as follows: a laser beam (pump beam) tuned to the absorption line of the species being investigated passes through the medium. If the non-radiative decay rate of the excited state (quenching rate in the case of vapors) is much faster than the radiative rate, then most of the optically absorbed energy appears in the thermal modes of the medium. This results in a change of the refractive index of the laser-irradiated region. This change in refractive index can be detected by a second, weaker laser beam (probe beam) in several different ways [2]. In this paper we limit ourselves to one method only, in which the refractive-index change is monitored by observing the deflection of the probe beam. The probe beam gets deflected, much like in the mirage effect, by the refractive-index gradient produced by the absorption of the pump beam. The technique can be used either with a cw pump beam or a pulsed pump beam. In this paper we only consider pulsed excitation of the species, because it is easier to obtain high peak powers required for two-photon excitation by pulsed lasers. The amplitude of the PTDS signal gives the concentration of the absorbing species. If it can be assumed that almost all of the absorbed optical energy from the pump beam ends up in the thermal modes of the medium, then absolute concentrations can be measured without using any kind of a calibration procedure. Moreover, the thermal transport properties of the medium can be deduced from the temporal evolution of the PTDS signal after the laser pulse is over. If the medium is flowing, the heated region of the medium travels downstream with the flow, which causes a deflection of the probe beam placed slightly downstream from the pump beam. The time of flight of the heat pulse between the pump and probe beams yields the flow velocity of the medium. In order to be able to obtain quantitative measurements of parameters such as species concentration, thermal transport properties, and flow velocity from the analysis of PTDS signals, it is necessary to have a complete theory of the generation and temporal evolution of the signals. We have recently demonstrated measurement of the absolute concentration of OH in a methane–oxygen flame [3], and a simultaneous measurement (from the analysis of a single data curve) of absolute OH concentration, temperature (which was de-

✉ Fax: +1-479/575-4580, E-mail: rgupta@uark.edu

rived from the measured value of thermal diffusivity), and flow velocity [4] in a H_2/O_2 flame using PTDS. Combustion, even that of a simple hydrocarbon, is a very complicated and poorly understood phenomenon. Measurements such as these may prove to be very valuable in determining if a particular model of combustion is correct. Of particular importance in the combustion process is the role played by atomic species, such as H and O, because they are extremely reactive and have fast diffusion rates. However, these atomic species cannot be measured by single-photon excitation, because their absorption lines lie in the vacuum-UV region of the spectrum. PTDS, in conjunction with two-photon excitation, provides a convenient way of measuring these species. Recently, it has been suggested [5] that PTDS may also be useful in the diagnostics of reacting low-temperature atmospheric-pressure plasmas, where conditions similar to those in combustion may exist. These are just two examples where two-photon PTDS may be useful. For quantitative analysis of the two-photon PTDS data, a rigorous theory of the generation and temporal evolution of the two-photon PTDS signal must be available. This is what is presented in this paper and we show below that there are substantial differences between the amplitudes (even for equal excitation rates), spatial profiles, and temporal evolutions of the one-photon and two-photon PTDS signals.

Previous experimental work on two-photon photothermal spectroscopy consists mainly of the measurement of the two-photon excitation spectrum [6–8] or absorption coefficient [9–12] in various liquids and solids. In almost all of the previous work a comprehensive theory of the generation and temporal evolution of the signal was not required, because either the relative values were measured (such as for the measurement of the spectrum) or the absorption coefficient was treated as a measured parameter proportional to the amplitude of the signal. The theory of two-photon (as a matter of fact, multiphoton) photothermal lensing spectroscopy was developed by Twarowski and Kliger [13] and, more recently, by Kamada et al. [14]. The theory presented here is considerably more general than that of [13, 14] as follows: (1) we have allowed for the possibility that the medium may be flowing. Of course, the special case of a stationary medium may be obtained by simply setting the flow velocity equal to zero. The measurement of thermal transport properties (and consequently that of the temperature) depends critically on the temporal evolution of the PTDS signal [3, 4, 15], and the temporal evolution is drastically influenced by the flow velocity. As a matter of fact, the signal shape in the presence of the flow is completely different from that in the absence of it. Moreover, if flow velocity is one of parameters to be measured, one must be able to predict the exact shape of the signal as a function of time. Therefore, inclusion of the possibility of a flow in the theory is critically important for applications such as plasma and combustion diagnostics but may also be important for some applications to liquids. (2) The previous authors have only considered very short optical pulses, which, in most cases, is a very good approximation. We have, however, considered an arbitrary pulse length. In some situations, it may be important to use long laser pulses. For example, if the two-photon transition probability is high then the transition could be easily saturated. This not only leads to complications in the signal analysis, but also limits the available signal-to-noise ratio (SNR). In these cases, it is better to use a long laser pulse with low peak power. Orders of magnitude improvement in SNR can be obtained. (3) While Twarowski and Kliger's theory allows for taking into account the temporal profile of the laser pulse, Kamada et al. assumed a rectangular pulse. This changes the result by a factor by $\sqrt{2}$ from that obtained by a more realistic Gaussian profile, even for a very short pulse. A systematic error of $\sim 30\%$ may not be acceptable in many cases. Our theory takes the temporal profile of the laser pulse explicitly into account. (4) We have taken line-width effects explicitly into account. In atomic and molecular vapors, the Doppler width may be important in many situations and, for two-photon excitation, the Doppler width depends on whether the laser beams co-propagate or counter-propagate. (5) The previous authors have treated the two-photon absorption cross section (or absorption coefficient) as a parameter in their theory. We have, on the other hand, expressed the absorption coefficient explicitly in terms of atomic oscillator strengths, polarization of the light, and Clebsch–Gordan coefficients. Thus, it would be possible to obtain absolute values of the density of absorbing species from the measured values of the absorption coefficients. Similar expressions may be developed for solids and liquids to express the two-photon absorption coefficient in terms of the known properties of those materials.

Expressions for the two-photon signal are derived in Sect. 2, and the theoretical results are discussed in Sect. 3. For brevity we have limited ourselves to photothermal deflection spectroscopy, but analogous expressions for photothermal lensing spectroscopy (thermal blooming) or photothermal phase-shift spectroscopy may be obtained by using the procedure outlined in [2].

2 Theory

In this section we derive the expressions for the generation and temporal evolution of the two-photon PTDS signals. In Sect. 2.1 to Sect. 2.4 we derive expressions for the two-photon transition probability, energy absorption, formation and evolution of the thermal image, and photothermal deflection signals, respectively.

2.1 *Two-photon transition probability*

In this subsection we derive expressions for the two-photon transition probability in explicit forms including the atomic line-width effects. Although most of the results given in this subsection are well known, putting all relevant expressions in one place for ready reference will help make this article self-contained.

Atoms (molecules) are excited from their ground state $|g\rangle$ to an excited state $|f\rangle$ of the same parity as the ground state by two photons of circular frequencies ω_1 and ω_2, such that the atomic frequency $\omega_{gf} = \omega_{gk} \pm \omega_{kf} = \omega_1 + \omega_2$, as shown in Fig. 1. The intermediate states $|k\rangle$ represent all atomic states of opposite parity, including the continuum states. The plus sign applies if the state $|k\rangle$ lies below the final state $|f\rangle$ whereas the negative sign applies if $|k\rangle$ is above $|f\rangle$.

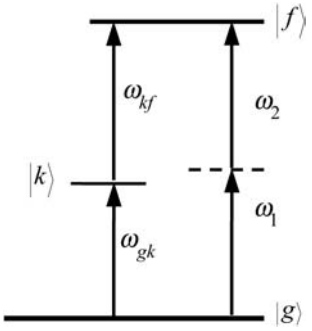

FIGURE 1 Energy levels involved in the two-photon absorption process

Our starting point is the well-known [16–18] expression for the two-photon transition probability $w^{(2)}$ between the atomic states $|g\rangle$ and $|f\rangle$,

$$w^{(2)} = \frac{(2\pi)^3}{(4\pi\varepsilon_0)^2\,\hbar^2 c^2}\left|P_{fg}^{(2)}\right|^2 I(\omega_1)I(\omega_2)g(\omega_1+\omega_2)\,. \tag{1}$$

Here $I(\omega_1)$ and $I(\omega_2)$ are, respectively, the intensities ($\mathrm{W/m^2}$) of radiation at frequencies ω_1 and ω_2, and $g(\omega_1+\omega_2)$ is the Lorentzian line-shape function

$$g(\omega_1+\omega_2) = \frac{\Delta\omega_{\mathrm{H}}/2\pi}{\left[\omega_{fg}-(\omega_1+\omega_2)\right]^2+\frac{\Delta\omega_{\mathrm{H}}^2}{4}}\,, \tag{2}$$

which has been normalized such that

$$\int g(\omega_1+\omega_2)\,\mathrm{d}(\omega_1+\omega_2) = 1\,. \tag{3}$$

Here $\Delta\omega_{\mathrm{H}}$ is the homogeneous line width (FWHM) of the transition. In (1), $P_{fg}^{(2)}$ is given by

$$\left|P_{fg}^{(2)}\right|^2 = \left|\sum_k \frac{\omega_{gk}\omega_{kf}}{\omega_1\omega_2}\left[\frac{\langle f\,|\hat{\boldsymbol{e}}_1\cdot\boldsymbol{D}|\,k\rangle\langle k\,|\hat{\boldsymbol{e}}_2\cdot\boldsymbol{D}|\,g\rangle}{E_{kg}-\hbar\omega_1}\right.\right.$$
$$\left.\left.+\frac{\langle f\,|\hat{\boldsymbol{e}}_2\cdot\boldsymbol{D}|\,k\rangle\langle k\,|\hat{\boldsymbol{e}}_1\cdot\boldsymbol{D}|\,g\rangle}{E_{kg}-\hbar\omega_2}\right]\right|^2\,, \tag{4}$$

where $\hat{\boldsymbol{e}}_1$ and $\hat{\boldsymbol{e}}_2$ are the polarization unit vectors of the two radiation fields, and $\boldsymbol{D}$ is the electric dipole moment operator of the atom. Equation (1) is valid when only the homogeneous broadening is present. In general Doppler broadening must also be considered. However, for two-photon absorption, the Doppler width depends on whether the two laser beams are co-propagating or counter-propagating, and whether the two optical frequencies are equal or unequal. Expressions for $g(\omega_1+\omega_2)$ appropriate for various cases are derived in the Appendix.

Equation (4) is purely a formal expression. In order for it to be useful, one must express it in terms of atomic oscillator strengths, which can be readily looked up in standard tables. For convenience, we have made the simplifying assumption that a single laser beam is used to excite the atoms, that is $\omega_1=\omega_2=\omega$, and that only one intermediate state $|k\rangle$ makes a significant contribution to the transition probability. We also use the standard results from the quantum theory of atoms [19]:

$$\left|\langle f\,|\hat{\boldsymbol{e}}_q\cdot\boldsymbol{D}|\,k\rangle\right|^2 = \frac{3e^2\hbar}{2m\omega_{kf}}f_{kf}\left|C(J_k1J_f;m_kqm_f)\right|^2\,, \tag{5}$$

where $\hat{\boldsymbol{e}}_q$ is the polarization unit vector of the light, expressed in terms of the spherical tensor components ($q=+1$ for σ_+ light, $q=-1$ for σ_- light, and $q=0$ for π light), f_{kf} is the oscillator strength of the $|k\rangle\rightarrow|f\rangle$ transition, and C is the Clebsch–Gordan coefficient in Rose's [20] notation. Equation (1), using (4) and (5), can then be written as

$$w^{(2)} = \frac{9\pi e^4}{2\varepsilon_0^2 m^2\hbar^2c^2}\frac{1}{\omega^4}\frac{\omega_{kf}\omega_{gk}}{\Delta\omega_k^2}f_{kf}f_{gk}$$
$$\times\left|C(J_k1J_f;m_kqm_f)\times C(J_g1J_k;m_gqm_k)\right|^2 I^2(\omega)g(2\omega), \tag{6}$$

where $g(2\omega)$ is given by (A.10) and $\Delta\omega_k=\omega_{gk}-\omega$.

2.2 *Energy absorption*

In this subsection we derive an expression for the absorption of power per unit volume, $Q^{(2)}$, as the laser beam propagates through the medium. We assume that the intensity of the radiation is not high enough to saturate the transition. We further assume that the medium is optically thin, that is, the attenuation of the laser beam is negligible as it propagates through the medium. Then

$$Q^{(2)} = 2\hbar\omega N_0 w^{(2)}\,, \tag{7}$$

where N_0 is the number density of atoms in the ground state that are available for excitation. The factor of two arises from the fact that two photons are absorbed in each transition. We rewrite (7) as

$$Q^{(2)}(r,\omega,t) = \beta(\omega)I^2(r,\omega,t)\,, \tag{8}$$

where, for convenience, we have defined β as

$$\beta(\omega) = \frac{2\hbar\omega N_0 w^{(2)}}{I^2}\,. \tag{9}$$

In (8), r is the radial coordinate (radial distance from the axis of the laser beam) and t is time. For pulsed-laser excitation, $I(r,t)$ explicitly depends on time. We assume that the laser intensity has both a Gaussian spatial profile and a Gaussian temporal profile:

$$I(r,\omega,t) = \frac{2E_0}{\pi a^2 t_0}\mathrm{e}^{-2r^2/a^2}\mathrm{e}^{-\pi(t-t')^2/t_0^2}\,, \tag{10}$$

where E_0 is the total energy in the laser pulse and a is the e^{-2}-radius of the laser beam. The Gaussian temporal profile is centered at time t' and has a temporal width (FWHM) of $2\sqrt{(\ln 2/\pi)}t_0 = 0.94t_0$. We have chosen this particular temporal width for the laser pulse, because this yields the same integrated energy as a rectangular pulse of width t_0.

2.3 *Formation and evolution of the thermal image*

In this subsection, we derive an expression for the temperature change produced by the absorption of the laser beam, and its subsequent temporal evolution due to thermal diffusion, and forced convection if present. We need to solve the following differential equation [2]:

$$\frac{\partial T^{(2)}(r,t)}{\partial t} = D\nabla^2 T^{(2)}(r,t) - v_x \frac{\partial T^{(2)}(r,t)}{\partial x} + \frac{1}{\varrho C_\mathrm{p}} Q^{(2)}(r,t)\,, \tag{11}$$

where $T^{(2)}(r,t)$ is the temperature of the medium above the ambient, and D, ϱ, and C_p are, respectively, the thermal diffusivity constant, density, and specific heat at constant pressure of the medium. For generality, we have assumed that the medium may be flowing, and for convenience we have assumed that the velocity, v_x, is entirely in the x direction. Results for the special case of a stationary medium are obtained by simply setting $v_x = 0$ in the final results. The source term $Q^{(2)}(r,t)$ is given by

$$Q^{(2)}(r,t) = \frac{4E_0^2\beta}{\pi^2 a^4 t_0^2} \mathrm{e}^{-4r^2/a^2} \mathrm{e}^{-2\pi(t-t')^2/t_0^2}\,, \tag{12}$$

where we have used (8) and (10) and suppressed the dependence of β on the laser frequency ω for brevity. Implicit in (11) is the assumption that all of the optical energy appears in the thermal (rotational–translational) modes of the medium on a very short time scale compared to the thermal diffusion and forced-convection times. This is generally true for fluid media at atmospheric pressure. Further, we assume that 100% of the absorbed optical energy appears in the thermal modes of the medium. If that is not the case, one only needs to scale the final result for $T^{(2)}(r,t)$ by a factor that depends on the fraction of energy transfer. We assume that the laser beam propagates in the z direction. Our assumption of the medium being optically thin implies that the temperature $T^{(2)}(r,t)$ is independent of the z coordinate. Therefore, we only need to solve (11) in two dimensions, x and y. If the medium is optically thick, then the treatment given here can easily be modified to take into account the z dependence of the temperature by the method used by He et al. [21] for the single-photon PTDS.

In order to solve (11), we have followed the Green's function method used earlier by Rose et al. [22] for the single-photon PTDS. Rose et al. assumed that the laser pulse's temporal profile was rectangular, that is, the laser pulse turned on sharply at $t = 0$ and turned off sharply at $t = t_0$, with the total energy in the pulse being E_0. The temporal profile of the pulse does not matter in that case as long as the laser pulse duration is so short that no significant thermal diffusion or forced convection takes place while the pulse is on. This condition is generally true in most experiments. However, for two-photon PTDS, one must take the temporal profile of the laser pulse explicitly into account even if the laser pulse is very short. The reason for this is as follows: the absorption of the laser energy in the case of two-photon excitation is proportional to $\beta(\omega)I^2(r,t)$, in other words, the absorption coefficient is proportional to $\beta(\omega)I(r,t)$. This means that the absorption coefficient itself depends on the temporal profile of the laser pulse, unlike the single-photon case where the absorption coefficient of the medium is independent of the laser pulse. The result is that the total energy absorbed explicitly depends on the temporal profile of the pulse. Following a procedure similar to that of Rose et al., with the modification of the source term as described above which includes the explicit time dependence of the laser pulse, we obtain for the thermal profile

$$\begin{aligned} T^{(2)}(x,y,t) = {} & \frac{4\beta E_0^2}{\pi^2 a^2 t_0^2 \varrho C_\mathrm{p}} \int_0^t \frac{1}{16D(t-\tau)+a^2} \\ & \times \mathrm{e}^{-4\left[(x-v_x(t-\tau))^2+y^2\right]\Big/\left[16D(t-\tau)+a^2\right]} \\ & \times \mathrm{e}^{-2\pi(\tau-t')^2/t_0^2}\,\mathrm{d}\tau\,, \end{aligned} \tag{13}$$

where the explicit expression for β is

$$\begin{aligned} \beta(\omega) = {} & N_0 \frac{9\pi e^4}{\varepsilon_0^2 m^2 \hbar c^2} \frac{1}{\omega^3} \frac{\omega_{kf}\omega_{gk}}{\Delta\omega_k^2} f_{kf} f_{gk} \\ & \times \left| C(J_k 1 J_f; m_k q m_f) C(J_g 1 J_k; m_g q m_k) \right|^2 g(2\omega)\,. \end{aligned} \tag{14}$$

Here we have used (6) and (9) and $g(2\omega)$ is given by (A.10). Equation (13) appears similar to the corresponding equation for the single-photon PTDS, but there are significant differences, which are important for quantitative analysis, and will be discussed in Sect. 3. This equation must be evaluated numerically. In this integration, t' must be chosen to be sufficiently large compared to t_0, so that most of the energy under the tail of the Gaussian is taken into account. Note that (13) is valid for any arbitrary pulse length.

In the special case where the laser pulse is very short compared to the thermal diffusion and forced-convection times, an analytical expression for $T^{(2)}(x,y,t)$ can be obtained as follows; first note that

$$\int_0^t \mathrm{e}^{-2\pi(\tau-t')^2/t_0^2}\,\mathrm{d}\tau = \frac{t_0}{\sqrt{2}}$$

if $t \gg t'$ and $t' \gg t_0$. Therefore, for the conditions under consideration, we may replace $\mathrm{e}^{-2\pi(\tau-t')^2/t_0^2}$ by the delta function $(t_0/\sqrt{2})\delta(\tau-t')$. Substituting this in (13), and then setting $t' = 0$ for simplicity, results in a very simple expression:

$$\begin{aligned} T^{(2)}(x,y,t) = {} & \frac{1}{\sqrt{2}} \frac{4\beta E_0^2}{\pi^2 a^2 t_0 \varrho C_\mathrm{p}} \\ & \times \frac{1}{16Dt+a^2} \mathrm{e}^{-4\left[(x-v_x t)^2+y^2\right]\Big/\left[16Dt+a^2\right]}\,. \end{aligned} \tag{15}$$

Equation (15) is an excellent approximation to (13) under most experimental conditions. Note that the factor of $1/\sqrt{2}$ arises from considering the temporal profile of the laser pulse explicitly.

2.4 *Photothermal deflection signals*

In this subsection we derive expressions for the deflection of a probe beam passing through a medium in which

the pump beam has created a refractive-index gradient due to a temperature change. We consider three cases: transverse PTDS, in which the probe beam travels in a direction perpendicular to the pump beam as shown in Fig. 2a, collinear PTDS, in which the probe beam travels in the same direction as the pump beam, as shown in Fig. 2b, and the general case where the probe beam may make an arbitrary angle with the pump beam, as shown in Fig. 2c. In all cases the probe beam may be displaced with respect to the pump beam in the x direction. In the following we treat the three cases individually.

2.4.1 Transverse PTDS. The PTDS signal $\varphi_{\mathrm{T}}(x,t)$ is given by [22]

$$\varphi_{\mathrm{T}}(x,t) = \frac{1}{n_0}\frac{\partial n}{\partial T}\int_{-\infty}^{\infty}\frac{\partial T(x,y,t)}{\partial x}\,\mathrm{d}y\,, \tag{16}$$

where n_0 is the ambient refractive index and $\partial n/\partial T$ is the temperature gradient of the refractive index. Use of (13) in (16) gives

$$\varphi_{\mathrm{T}}^{(2)}(x,t) = -\frac{1}{n_0}\frac{\partial n}{\partial T}\frac{16\beta E_0^2}{\pi^{3/2}a^2t_0^2\varrho C_{\mathrm{p}}}\int_0^t\frac{x-v_x(t-\tau)}{\left[16D(t-\tau)+a^2\right]^{3/2}} \times \mathrm{e}^{-4(x-v_x(t-\tau))^2/\left[16D(t-\tau)+a^2\right]}\mathrm{e}^{-2\pi(\tau-t')^2/t_0^2}\,\mathrm{d}\tau\,. \tag{17}$$

For the special case of a very short optical pulse, (17) reduces to an analytical expression:

$$\varphi_{\mathrm{T}}^{(2)}(x,t) = -\frac{1}{n_0}\frac{\partial n}{\partial T}\frac{16\beta E_0^2}{\sqrt{2}\pi^{3/2}a^2t_0\varrho C_{\mathrm{p}}}\frac{x-v_xt}{\left[16Dt+a^2\right]^{3/2}} \times \mathrm{e}^{-4(x-v_xt)^2/\left[16Dt+a^2\right]}. \tag{18}$$

2.4.2 Collinear PTDS. In this case the deflection angle $\varphi_{\mathrm{L}}(x,y,t)$ is given by [22]

$$\varphi_{\mathrm{L}}(x,y,t) = \frac{1}{n_0}\frac{\partial n}{\partial T}\int_0^l\frac{\partial T(x,y,t)}{\partial x}\,\mathrm{d}z\,, \tag{19}$$

where l is the length of the medium. Substitution of (13) in (19) results in

$$\varphi_{\mathrm{L}}^{(2)}(x,y,t) = -\frac{l}{n_0}\frac{\partial n}{\partial T}\frac{32\beta E_0^2}{\pi^2a^2t_0^2\varrho C_{\mathrm{p}}}\int_0^t\frac{x-v_x(t-\tau)}{\left[16D(t-\tau)+a^2\right]^2} \times \mathrm{e}^{-4\left[(x-v_x(t-\tau))^2+y^2\right]/\left[16D(t-\tau)+a^2\right]} \times \mathrm{e}^{-2\pi(\tau-t')^2/t_0^2}\mathrm{d}\tau\,. \tag{20}$$

For a very short optical pulse, this equation reduces to

$$\varphi_{\mathrm{L}}^{(2)}(x,y,t) = -\frac{l}{n_0}\frac{\partial n}{\partial T}\frac{32\beta E_0^2}{\sqrt{2}\pi^2a^2t_0\varrho C_{\mathrm{p}}}\frac{x-v_xt}{\left[16Dt+a^2\right]^2} \times \mathrm{e}^{-4\left[(x-v_xt)^2+y^2\right]/\left[16Dt+a^2\right]}. \tag{21}$$

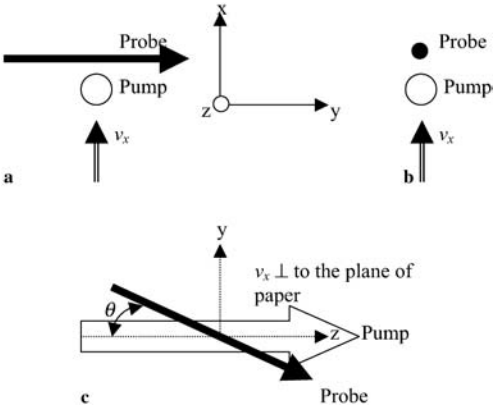

FIGURE 2 Pump- and probe-beam configurations for **a** transverse PTDS, **b** collinear PTDS, and **c** when the pump and probe beams make an arbitrary angle θ with respect to each other

2.4.3 Arbitrary angle. Now we consider the general case where the probe beam may make any arbitrary angle θ with the pump beam, as shown in Fig. 2c. Following a procedure similar to that of Rose et al. [22], we find that

$$\varphi^{(2)}(x,\theta,t) = -\frac{1}{n_0}\frac{\partial n}{\partial T}\frac{16\beta E_0^2}{\pi^{3/2}a^2t_0^2\varrho C_{\mathrm{p}}\sin\theta} \times\int_0^t\frac{x-v_x(t-\tau)}{\left[16D(t-\tau)+a^2\right]^{3/2}} \times \mathrm{e}^{-4(x-v_x(t-\tau))^2/\left[16D(t-\tau)+a^2\right]}\,\mathrm{e}^{-2\pi(t-t')^2/t_0^2}\,\mathrm{d}\tau\,, \tag{22}$$

for $\pi/2 \geq \theta \geq 2\theta_0$, and for $0 \leq \theta \leq \theta_0$ an approximate simple expression may be written as

$$\varphi^{(2)}(x,\theta,t) = -\frac{l}{n_0}\frac{\partial n}{\partial T}\frac{32\beta E_0^2}{\pi^2a^2t_0^2\varrho C_{\mathrm{p}}\cos\theta} \times\int_0^t\frac{x-v_x(t-\tau)}{\left[16D(t-\tau)+a^2\right]^2} \times \mathrm{e}^{-4(x-v_x(t-\tau))^2/\left[16D(t-\tau)+a^2\right]}\mathrm{e}^{-2\pi(t-t')^2/t_0^2}\,\mathrm{d}\tau\,, \tag{23}$$

where the angle θ_0 is defined [22] by $\theta_0 \approx \tan^{-1}\left(\sqrt{2(a^2+16Dt)}/l\right)$. In the intermediate region, $\theta_0 < \theta < 2\theta_0$, no simple approximate expression can be written and an exact expression involving a double integral must be derived using the procedure outlined in [22].

For the short optical pulse, (22) and (23) may be simplified, respectively, to

$$\varphi^{(2)}(x,\theta,t) = -\frac{1}{n_0}\frac{\partial n}{\partial T}\frac{16\beta E_0^2}{\sqrt{2}\pi^{3/2}a^2t_0\varrho C_{\mathrm{p}}} \times\frac{x-v_xt}{\left[16Dt+a^2\right]^{3/2}\sin\theta}\mathrm{e}^{-4(x-v_xt)^2/[16Dt+a^2]} \tag{24}$$

for $\pi/2 \geq \theta \geq 2\theta_0$ and

$$\varphi^{(2)}(x,\theta,t) = -\frac{l}{n_0}\frac{\partial n}{\partial T}\frac{32\beta E_0^2}{\sqrt{2}\pi^2 a^2 t_0 \varrho C_\mathrm{p}} \times \frac{x - v_x t}{\left[16Dt + a^2\right]^2 \cos\theta} \mathrm{e}^{-4(x-v_x t)^2/\left[16Dt+a^2\right]} \tag{25}$$

for $0 \leq \theta \leq \theta_0$.

3 Results and discussion

In this section we discuss the implications of the expressions for the temperature profile and the PTDS signals derived in Sect. 2. In order to highlight the important features of two-photon PTDS, it is useful to compare the two-photon signals with the one-photon signals. This comparison is more transparent if we recast the expressions in terms of the energy absorbed by the medium per unit path length of the pump beam, u_1. For the single-photon case,

$$u_1^{(1)} = \int_0^\infty \int_0^\infty Q^{(1)}(r,t) 2\pi r \,\mathrm{d}r \,\mathrm{d}t = \alpha E_0 \,, \tag{26}$$

where $Q^{(1)}(r,t)$ is the power absorbed by the medium per unit volume ((2) of [22]), α is the absorption coefficient of the medium, E_0 is the laser pulse energy, and a Gaussian spatial profile for the pump beam is assumed. For the two-photon case,

$$u_1^{(2)} = \int_0^\infty \int_0^\infty Q^{(2)}(r,t) 2\pi r \,\mathrm{d}r \,\mathrm{d}t = \frac{\beta E_0^2}{\sqrt{2}\pi a^2 t_0} \,, \tag{27}$$

where we have used (8) and (10). In the following, we compare the temperature profiles and the PTDS signals for the two cases assuming that the energy absorbed per unit length is the same in both cases, that is $u_1^{(1)} = u_1^{(2)}$. We discuss below first the temperature profile, and then the PTDS signals. For the sake of simplicity we only consider the results in the short-pulse approximation and only for the transverse PTDS. In order to illustrate the results, we have chosen an arbitrary but realistic example: PTDS signals generated by two-photon excitation of the $5\,^2D_{3/2}$ state of Rb vapor in a cell containing 500 Torr of N_2 as the quenching gas.

3.1 *Temperature profile*

Equation (15) can be rewritten in terms of $u_1^{(2)}$ as

$$T^{(2)}(x,y,t) = \frac{4u_1^{(2)}}{\pi\varrho C_\mathrm{p}\left[16Dt + a^2\right]} \mathrm{e}^{-4\left[(x-v_x t)^2 + y^2\right]/\left[16Dt+a^2\right]} \,. \tag{28}$$

The analogous expression for the single-photon case ((36) of [22]) can be written as

$$T^{(1)}(x,y,t) = \frac{2u_1^{(1)}}{\pi\varrho C_\mathrm{p}\left[8Dt + a^2\right]} \mathrm{e}^{-2\left[(x-v_x t)^2 + y^2\right]/\left[8Dt+a^2\right]} \,. \tag{29}$$

We note that at $x = y = 0$ and $t = 0$, $T^{(2)} = 2T^{(1)}$. The explanation for this is simple: for the two-photon case, the thermal energy is distributed over a narrower radial profile than it is for the single-photon case; therefore, the peak temperature $T^{(2)}$ is higher than the peak temperature $T^{(1)}$.

Figures 3 and 4 show the temperature profiles at various times after the laser pulse is over, for a stationary medium and a medium with a flow velocity of 1 m/s, respectively. $T^{(2)}(x,y,t)/2$ is plotted (solid lines) as a function of the ratio of x coordinate and the beam radius. y was set equal to zero for convenience. In this calculation, we assumed that $u_1^{(2)} = 80\,\mu\mathrm{J/cm}$, appropriate for the $5\,^2S_{1/2} \rightarrow 5\,^2D_{3/2}$ two-photon transition of Rb at 777.97 nm ($\beta = 3.4 \times 10^{-8}$ ms/J), $a = 1$ mm, $E_0 = 100\,\mu$J, and $t_0 = 10$ ns. The sample cell was

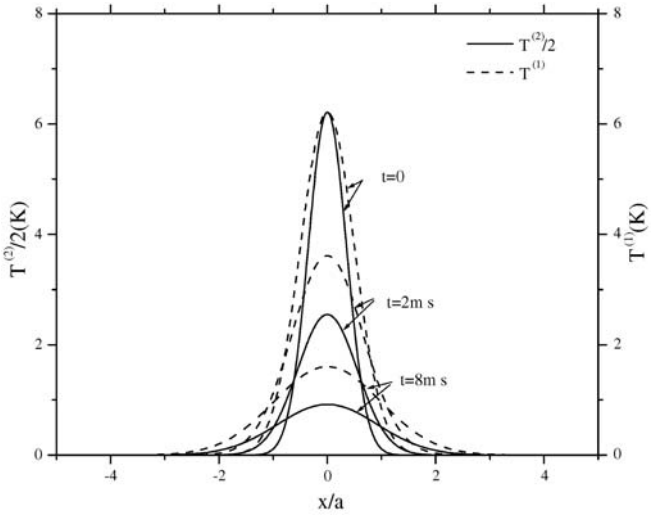

FIGURE 3 Spatial profile of the heat pulse produced by two-photon excitation of the $5\,^2D_{3/2}$ state of Rb, $T^{(2)}$, in a stationary medium, 0, 2 ms, and 8 ms after the laser pulse (*solid lines*). The *dashed lines* show $T^{(1)}$, the thermal profile produced by single-photon excitation of Rb vapor, with an equal amount of energy absorption per unit length. The temperature is plotted against the radial distance from the axis of the pump beam, measured in units of the pump-beam radius. Values of the parameters used in this calculation are given in the text

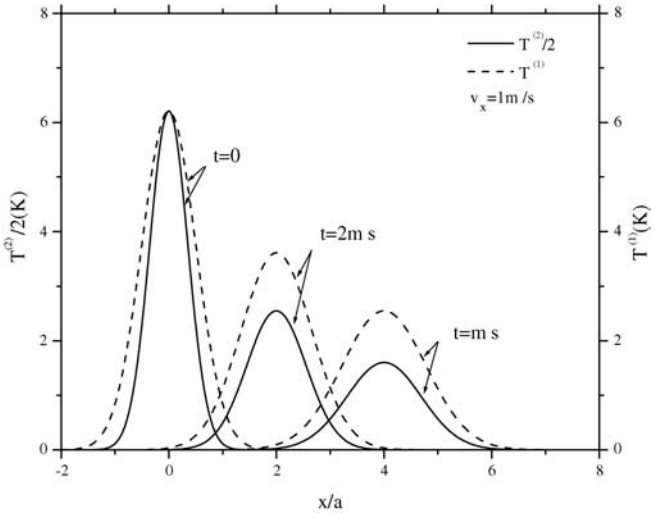

FIGURE 4 Temperature profiles, $T^{(2)}$ and $T^{(1)}$, produced by two-photon and single-photon excitation, respectively, with equal energy absorption per unit length in a medium flowing with a velocity of 1 m/s. Parameters used in this calculation are the same as those in Fig. 3

assumed to have been heated to $T = 470\,\mathrm{K}$, with a corresponding Rb vapor pressure of 0.8×10^{-1} Torr. We used $D = 4.49 \times 10^{-5}\,\mathrm{m^2/s}$ and $\varrho C_\mathrm{p} = 820\,\mathrm{J/m^3K}$, appropriate for N_2 at 500 Torr. The figures show that at $t = 0$ the temperature profile is a Gaussian with a e^{-2}-radius of $a/\sqrt{2}$, and it broadens due to the diffusion of heat as the time progresses. In addition, if the medium is flowing, the thermal profile moves downstream with the fluid flow while it broadens due to thermal diffusion. For comparison we have also shown $T^{(1)}(x, y, t)$ calculated using (29) and $u_1^{(1)} = 80\,\mu\mathrm{J/cm}$ (dashed curves). In this comparison we note two things: (a) at $t = 0$ the thermal profile of $T^{(2)}$ is narrower than that of $T^{(1)}$ because of the quadratic dependence of $T^{(2)}$ on the laser intensity. (b) The rate of diffusion of heat in the two-photon thermal profile is twice as fast as it is in the single-photon thermal profile. This is due to a higher spatial gradient of the $T^{(2)}$ thermal profile. The consequences of these differences on the PTDS signals will be apparent below.

3.2 *PTDS signals*

Equation (18) for $\varphi_\mathrm{T}^{(2)}$ may be rewritten in terms of $u_1^{(2)}$ as

$$\varphi_\mathrm{T}^{(2)}(x,t) = -\frac{1}{n_0}\frac{\partial n}{\partial T}\frac{16u_1^{(2)}}{\sqrt{\pi}\varrho C_\mathrm{p}}\frac{x - v_x t}{\left[16Dt + a^2\right]^{3/2}} \times \mathrm{e}^{-4(x-v_x t)^2/\left[16Dt+a^2\right]}. \tag{30}$$

The corresponding equation for $\varphi_\mathrm{T}^{(1)}$ ((38) of [22]) is

$$\varphi_\mathrm{T}^{(1)}(x,t) = -\frac{1}{n_0}\frac{\partial n}{\partial T}\frac{8u_1^{(1)}}{\sqrt{2\pi}\varrho C_\mathrm{p}}\frac{x - v_x t}{\left[8Dt + a^2\right]^{3/2}} \times \mathrm{e}^{-2(x-v_x t)^2/\left[8Dt+a^2\right]}. \tag{31}$$

Figure 5 shows $\varphi_\mathrm{T}^{(2)}(x)/2$ at $t = 0$ (solid curve) as a function of the radial distance from the pump-beam axis measured in units of the pump-beam radius for a stationary medium. For comparison, the single-photon PTDS signal $\varphi_\mathrm{T}^{(1)}(x)$ is shown by the dashed line. $u_1^{(2)}$ has been set equal to $u_1^{(1)}$, and all parameters have the same values as those for Figs. 3 and 4. The deflection is plotted in microradians. Note that the profile of $\varphi_\mathrm{T}^{(2)}(x)$ is narrower than that of $\varphi_\mathrm{T}^{(1)}(x)$, its peak occurs at $x = a/2\sqrt{2}$ while that of $\varphi_\mathrm{T}^{(1)}(x)$ occurs at $x = a/2$, and the peak value of $\varphi_\mathrm{T}^{(2)}(x)$ is a factor of two higher than that of $\varphi_\mathrm{T}^{(1)}(x)$. The physical reasons for this factor of two are as follows: a factor of two arises from the fact that $T^{(2)}$ is higher than $T^{(1)}$, and another factor of two arises from the larger spatial gradient of $T^{(2)}$. For transverse PTDS, the path length traversed by the probe beam through the thermal profile is a factor of $1/\sqrt{2}$ shorter for $\varphi_\mathrm{T}^{(2)}$ than it is for $\varphi_\mathrm{T}^{(1)}$ because of the differences in the widths of the thermal profiles. Finally, the peak value of $\varphi_\mathrm{T}^{(2)}$ occurs at $x = a/2\sqrt{2}$ rather than at $x = a/2$, which reduces its peak value further by a factor of $1/\sqrt{2}$. These four factors combine to give a factor of two.

Finally, Figs. 6 and 7 show the temporal evolution of $\varphi_\mathrm{T}^{(2)}$ and $\varphi_\mathrm{T}^{(1)}$ for a stationary medium and a medium with $v_x = 1\,\mathrm{m/s}$, respectively. Again, both $\varphi_\mathrm{T}^{(2)}$ and $\varphi_\mathrm{T}^{(1)}$ have been evaluated using the same parameters as those used for Fig. 3. In Fig. 6, $\varphi_\mathrm{T}^{(2)}$ has been evaluated at $x = a/2\sqrt{2}$ whereas $\varphi_\mathrm{T}^{(1)}$ has been evaluated at $x = a/2$ to make the comparison of their temporal evolutions easier. Figure 7 is plotted for $x = 4a$. Both of these figures illustrate faster diffusion of heat in two-photon PTDS than it is in single-photon PTDS. As noted previously, this is a very important factor to recognize if the temporal evolution of the signal is to be used for measurement of thermal transport properties of the medium, or for the measurement of the temperature via the measurement of thermal transport parameters of the medium.

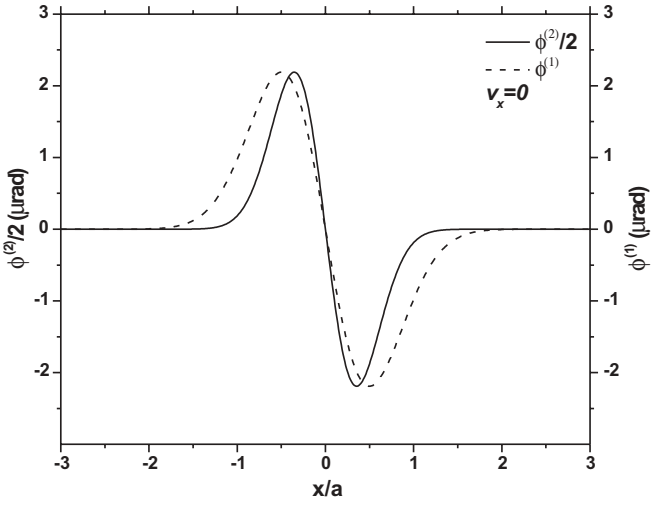

FIGURE 5 Photothermal deflection at $t = 0$, $\varphi_\mathrm{T}^{(2)}$ and $\varphi_\mathrm{T}^{(1)}$, produced by two-photon and single-photon excitation of Rb, respectively, in a stationary medium as a function of the distance from the axis of the pump beam. Both signals have been evaluated for equal amounts of energy absorption per unit length of the medium

In conclusion, we have presented a general theory of two-photon photothermal deflection spectroscopy applicable to

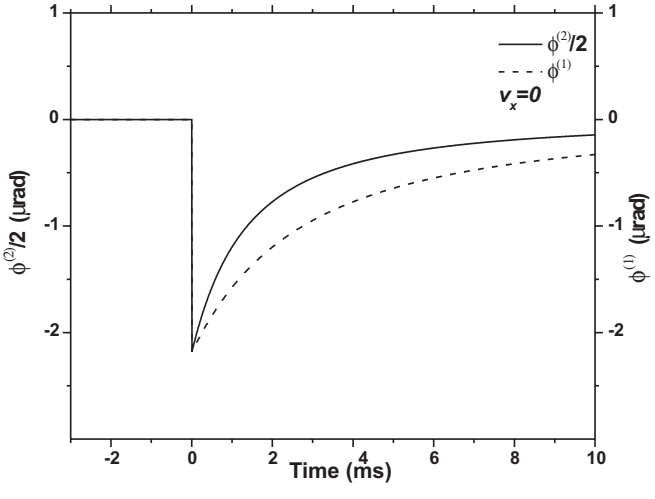

FIGURE 6 Temporal profile of the PTDS signal in a stationary medium. The two-photon PTDS signal, $\varphi_\mathrm{T}^{(2)}$, was evaluated at $x = a/2\sqrt{2}$ and the single-photon PTDS signal was evaluated at $x = a/2$, where their respective maximum values occur. The probe beam deflects sharply when the laser pulse is fired, and returns to its original position on a time scale characteristic of the thermal diffusion time

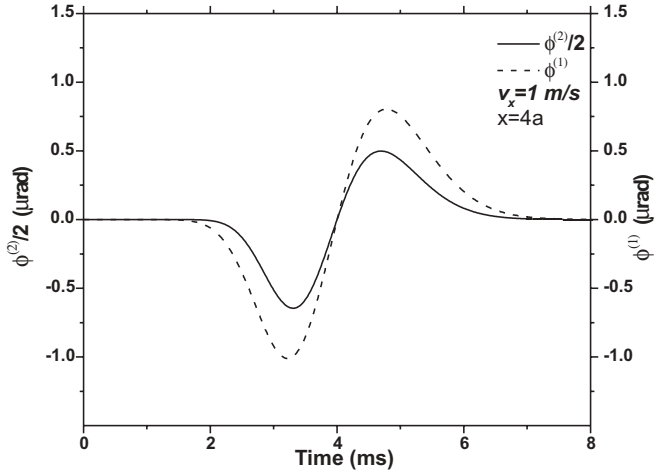

FIGURE 7 Temporal profiles of $\varphi_{\mathrm{T}}^{(2)}$ and $\varphi_{\mathrm{T}}^{(1)}$, the two-photon and single-photon PTDS signals, respectively, in a medium flowing with a flow velocity of 1 m/s. The temporal profile in this case consists of the gradient of a Gaussian broadened by thermal diffusion

both stationary and flowing media. The optical pulse may be arbitrarily long, and the optical pulse shape is explicitly taken into account. Doppler effects for co-propagating and counter-propagating beams are taken into account and, for atomic vapors, the results are expressed in terms of oscillator strengths and Clebsch–Gordan coefficients. It is shown that, for quantitative measurements, it is important to take the optical pulse shape into account, even for very short pulses. It is also shown that, for the same amount of energy absorption per unit length, the two-photon PTDS signal is larger than the single-photon PTDS signal. Finally, it is found that thermal diffusion affects the two-photon signal more than it does the single-photon signal.

Appendix: effect of Doppler broadening on two-photon absorption

Let us assume that the two laser beams have wave vectors $\boldsymbol{k}_1$ and $\boldsymbol{k}_2$, and the velocity of a particular atom is $\boldsymbol{v}$. This atom sees the two laser frequencies to be Doppler shifted by $\boldsymbol{v}\cdot\boldsymbol{k}_1$ and $\boldsymbol{v}\cdot\boldsymbol{k}_2$, and (4) and (2) are modified as follows:

$$P_{fg}^{(2)} = \sum_k \frac{\omega_{gk}\omega_{kf}}{(\omega_1+\boldsymbol{v}\cdot\boldsymbol{k}_1)\,(\omega_2+\boldsymbol{v}\cdot\boldsymbol{k}_2)} \cdot\left[\frac{\langle f\,|\hat{\boldsymbol{e}}_1\cdot\boldsymbol{D}|\,k\rangle\langle k\,|\hat{\boldsymbol{e}}_2\cdot\boldsymbol{D}|\,g\rangle}{\hbar\left[\omega_{kg}-(\omega_1+\boldsymbol{v}\cdot\boldsymbol{k}_1)\right]} + \frac{\langle f\,|\hat{\boldsymbol{e}}_2\cdot\boldsymbol{D}|\,k\rangle\langle k\,|\hat{\boldsymbol{e}}_1\cdot\boldsymbol{D}|\,g\rangle}{\hbar\left[\omega_{kg}-(\omega_2+\boldsymbol{v}\cdot\boldsymbol{k}_2)\right]}\right] \tag{A.1}$$

and

$$g(\omega_1+\omega_2) = \frac{\Delta\omega_{\mathrm{H}}/2\pi}{\left[\omega_{fg}-(\omega_1+\boldsymbol{v}\cdot\boldsymbol{k}_1)-(\omega_2+\boldsymbol{v}\cdot\boldsymbol{k}_2)\right]^2+\frac{\Delta\omega_{\mathrm{H}}^2}{4}}\,. \tag{A.2}$$

We would need to integrate the transition probability over the distribution of atomic velocities. However, in general, both ω_1 and ω_2 are far enough from the single-photon resonance frequency ω_{kg} that we may assume that $\omega_{kg}-\omega_1 \gg \boldsymbol{v}\cdot\boldsymbol{k}_1$ and $\omega_{kg}-\omega_2 \gg \boldsymbol{v}\cdot\boldsymbol{k}_2$ for almost all the atoms. For simplicity then we may assume that the effect of atomic velocities on (A.1) is negligible. On the other hand, (A.2) goes through a resonance at $\omega_{fg}\cong\omega_1+\omega_2$, and we need to consider this term in detail. In the following we will distinguish between two cases: the two beams are counter-propagating or co-propagating.

A.1 *Counter-propagating beams*

We assume that the two beams are counter-propagating in the z direction. We make a further distinction between the cases when the two optical frequencies are equal or unequal.

A.1.1 Unequal frequencies. We assume that the two optical frequencies, ω_1 and ω_2, are sufficiently different that it is not possible to excite the atoms by two-photon absorption from a single beam. In this case (A.2) becomes

$$g(\omega_1+\omega_2) = \frac{\Delta\omega_{\mathrm{H}}/2\pi}{\left[\omega_{fg}-(\omega_1+\omega_2)-\upsilon_z\,(k_1-k_2)\right]^2+\frac{\Delta\omega_{\mathrm{H}}^2}{4}}\,. \tag{A.3}$$

We must now integrate over the distribution of atomic velocities. Let us assume that there are N_0 atoms per unit volume in the sample. Then the number of atoms making transitions per unit time is

$$\frac{\mathrm{d}N_0}{\mathrm{d}t} = \int_{-\infty}^{\infty}\frac{\mathrm{d}N(\upsilon_z)}{\mathrm{d}t}\,\mathrm{d}\upsilon_z = \int_{-\infty}^{\infty} w^{(2)}(\omega_1,\omega_2,\upsilon_z)N(\upsilon_z)\,\mathrm{d}\upsilon_z\,, \tag{A.4}$$

where $N(\upsilon_z)\,\mathrm{d}\upsilon_z$ is the number of atoms with z component of their velocities between υ_z and $\upsilon_z+\mathrm{d}\upsilon_z$, irrespective of their x and y components of velocities, and in thermal equilibrium at a temperature T. $N(\upsilon_z)$ is given by

$$N(\upsilon_z)\,\mathrm{d}\upsilon_z = \frac{N_0}{\sqrt{\pi}\upsilon_0}\mathrm{e}^{-(\upsilon_z/\upsilon_0)^2}\,\mathrm{d}\upsilon_z\,, \tag{A.5}$$

where $\upsilon_0=(2kT/M)^{1/2}$. Using (1), (A.3), and (A.5) in (A.4) we conclude that when the Doppler effect is taken account for counter-propagating beams with unequal frequencies, the line-shape factor $g(\omega_1+\omega_2)$ is replaced by a new line-shape factor

$$g^{(-)}(\omega_1+\omega_2,T) = \frac{1}{\sqrt{\pi}\upsilon_0}\int_{-\infty}^{\infty}\frac{(\Delta\omega_{\mathrm{H}}/2\pi)\mathrm{e}^{-(\upsilon_z/\upsilon_0)^2}\,\mathrm{d}\upsilon_z}{\left[\omega_{fg}-(\omega_1+\omega_2)-\upsilon_z(k_1-k_1)\right]^2+\frac{\Delta\omega_{\mathrm{H}}^2}{4}}\,. \tag{A.6}$$

Equation (A.6) represents a Voigt profile, and it is the convolution of a Lorentzian with the homogeneous line width $\Delta\omega_{\mathrm{H}}$ and a Gaussian with a very small residual Doppler width.

Note that the Doppler width is reduced by a factor of $(\omega_1 - \omega_2)/(\omega_1 + \omega_2)$. This is because the Doppler shift of each atom with respect to the two counter-propagating photons nearly cancels out.

Note that when ω_1 is exactly equal to ω_2, the Doppler width is completely eliminated. However, in that case the Doppler-free signal sits on top of a broad background due to the absorption of both photons for a single beam, as explained below. It is possible to eliminate this broad background, however, by choosing the polarization of the beams in such a way that absorption of two photons from a single beam is not possible.

A.1.2 Equal frequencies. In this case the line-shape factor $g(\omega_1 + \omega_2)$ (A.2) has two terms:

$$g^{(-)}(\omega_1+\omega_2) = g^{(-)}(2\omega) = \frac{\Delta\omega_{\mathrm{H}}/2\pi}{\left[\omega_{fg}-2\omega\right]^2+\frac{\Delta\omega_{\mathrm{H}}^2}{4}} + \frac{\Delta\omega_{\mathrm{H}}/2\pi}{\left[\omega_{fg}-2\omega\pm 2\upsilon_z k\right]^2+\frac{\Delta\omega_{\mathrm{H}}^2}{4}}, \quad \text{(A.7)}$$

where the first term represents the Doppler-free line shape due to the absorption of one photon from each of the two counter-propagating beams. The second term represents the absorption of both photons from a single beam. The plus and the minus signs refer to the beams traveling in the negative and positive z directions, respectively. Averaging over the distribution of atomic velocities then leads to

$$g^{(-)}(2\omega) = \eta\frac{\Delta\omega_{\mathrm{H}}/2\pi}{\left[\omega_{fg}-2\omega\right]^2+\frac{\Delta\omega_{\mathrm{H}}^2}{4}} + (1-\eta)\frac{1}{\sqrt{\pi}\upsilon_0}\int_{-\infty}^{\infty}\frac{(\Delta\omega_{\mathrm{H}}/2\pi)\mathrm{e}^{-(\upsilon_z/\upsilon_0)^2}\,\mathrm{d}\upsilon_z}{\left[\omega_{fg}-2\omega-2\upsilon_z k\right]^2+\frac{\Delta\omega_{\mathrm{H}}^2}{4}}. \quad \text{(A.8)}$$

The first term in (A.5) is simply the Doppler-free Lorentzian profile discussed in Sect. A.1.1 above for the special case of $\omega_1 = \omega_2$. The second term is the Voigt profile, and it represents a broad Doppler-broadened background signal which arises due to the absorption of both photons from a single beam. Both the $+2\upsilon_z k$ and $-2\upsilon_z k$ terms contribute equally after integration over the atomic velocity distribution; therefore only one term has been included. In (A.8) the first and second terms have been normalized to η and $1-\eta$, respectively. These factors represent the relative number of atoms that lie within the Doppler-free profile and the Doppler-broadened background, respectively. By a proper of choice of polarizations of the two beams, η can be made equal to 1. In that case the Doppler background disappears. If the two beams have the same polarization and intensity, $\eta = 2/3$, that is, twice as many atoms are under the Doppler-free profile as there are under the Doppler background as shown by Grynberg and Cagnac [17].

A.2 *Co-propagating beams*

A.2.1 Unequal frequencies. Following a procedure similar to that used to derive (A.6), we find the profile in this case to be

$$g^{(+)}(\omega_1+\omega_2, T) = \frac{1}{\sqrt{\pi}\upsilon_0}\int_{-\infty}^{\infty}\frac{(\Delta\omega_{\mathrm{H}}/2\pi)\mathrm{e}^{-(\upsilon_z/\upsilon_0)^2}\,\mathrm{d}\upsilon_z}{\left[\omega_{fg}-(\omega_1+\omega_2)-\upsilon_z(k_1+k_1)\right]^2+\frac{\Delta\omega_{\mathrm{H}}^2}{4}}. \quad \text{(A.9)}$$

This is again a Voigt profile but, unlike (A.6), it represents a very broad line width.

A.2.2 Equal frequencies. This is simply a special case of (A.9) and the profile is given by

$$g^{(+)}(2\omega, T) = \frac{1}{\sqrt{\pi}\upsilon_0}\int_{-\infty}^{\infty}\frac{(\Delta\omega_{\mathrm{H}}/2\pi)\mathrm{e}^{-(\upsilon_z/\upsilon_0)^2}\,\mathrm{d}\upsilon_z}{\left[\omega_{fg}-2\omega-2\upsilon_z k\right]^2+\frac{\Delta\omega_{\mathrm{H}}^2}{4}}. \quad \text{(A.10)}$$

REFERENCES

1 See, for example, *Proc. 12th Int. Conf. Photoacoustic and Photothermal Phenomena* [Rev. Sci. Instrum. Part II **74**(1) (2003)]
2 See, for example, R. Gupta: in *Photothermal Investigations of Solids and Fluids*, ed. by J.A. Sell (Academic, New York 1989) Chap. 3
3 Y. Li, R. Gupta: Appl. Opt. **42**, 2226 (2003)
4 Y. Li, R. Gupta: Appl. Phys. B **75**, 903 (2002)
5 See, for example, R. Gupta: in *Proc. 11th Int. Symp. Laser-Aided Plasma Diagnostics, Les Houches, France, 2003* (unpublished)
6 A.J. Twarowski, D.S. Kliger: Chem. Phys. **20**, 259 (1977)
7 H.L. Fang, T.L. Gustafson, R.L. Swofford: J. Chem. Phys. **78**, 1663 (1983)
8 A. Kurian, S.T. Lee, K.P. Unnikrishnan, D.S. George, V.P.N. Nampoori, C.P.G. Vallabhan: J. Nonlinear Opt. Phys. Mater. **12**, 75 (2003)
9 W.T. White III, M.A. Henesian, M.J. Weber: J. Opt. Soc. Am. B **2**, 1402 (1985)
10 C. Halvorson, A.J. Heeger: Chem. Phys. Lett. **216**, 488 (1993)
11 Y. Han, J.S. Rosenshein, Z.L. Wu, W. Ye, M. Thomsen, Q. Zhao: Opt. Eng. **40**, 303 (2001)
12 B.C. Li, S. Martin, E. Welsch: in *Laser-Induced Damage in Optical Materials: 2000*, ed. by G.J. Exarhos, A.J. Guenther, M.R. Kozlowski, K.L. Lewis, M.J. Soileau (The International Society of Optical Engineering, Bellingham, WA, USA 2001) [Proc. SPIE **4347**, 82 (2001)]
13 A.J. Twarowski, D.S. Kliger: Chem. Phys. **20**, 253 (1977)
14 K. Kamada, K. Matsunaga, A. Yoshino, K. Ohta: J. Opt. Soc. Am. B **20**, 529 (2003)
15 Y. Li, R. Gupta: Appl. Phys. B **75**, 103 (2002)
16 A. Gold: in *Proc. Int. School of Physics, Course XLII, Quantum Optics*, ed. by R.J. Glauber (Academic, New York 1969)
17 G. Grynberg, B. Cagnac: Rep. Prog. Phys. **40**, 791 (1977); B. Cagnac, G. Grynberg, F. Biraben: J. Phys. (Paris) **34**, 845 (1973)
18 W. Bischel, P.J. Kelly, C.K. Rhodes: Phys. Rev. A **13**, 1817 (1976)
19 See, for example, B.W. Shore, D.H. Menzel: *Principles of Atomic Spectra* (Wiley, New York 1968)
20 M.E. Rose: *Elementary Theory of Angular Momentum* (Wiley, New York 1957)
21 Q. He, R. Vyas, R. Gupta: Appl. Opt. **36**, 1841 (1997)
22 A. Rose, R. Vyas, R. Gupta: Appl. Opt. **25**, 4626 (1986)